Electronic Supplementary Information

Experimental Section

Materials

Copper foil (CF), manganese acetate ($Mn(CH_3COO)_2$), anhydrous sodium sulfate (Na_2SO_4), sodium nitrate ($NaNO_3$), sodium nitrite ($NaNO_2$), ammonium chloride (NH_4Cl), 0.8 wt% sulfamic acid (H_3NO_3S), P-aminobenzenesulfonamide, N-(1-Naphthyl) ethylenediamine dihydrochloride, Nessler's reagent, and potassium sodium tartrate were purchased from Aladdin Chemical Reagent Co., Ltd. (Shanghai, China). $^{15}NH_4Cl$ and $Na^{15}NO_3$ were purchased from MacLin Biochemical Co., Ltd. (Shanghai, China). Hydrochloricacid (HCl) and phosphoric acid (H_3PO_4) were purchased from Tianjin Fengchuan Chemical Reagent Co, Ltd. All chemicals are analytical grade and used without further purification.

Synthesis of $Mn_3O_4/CuO_x/CF$

The CF was ultrasonically cleaned with acetone, ethanol, and deionized (DI) water for 5 min, respectively, and then dried with N_2 flow. Finally, the CF (1 × 2.5 cm^2) was calcined at 400 °C for 3 h under air atmosphere. The sample was gradually cooled down to room temperature for further use. Then an electrodeposition solution containing 55 mM manganese acetate and 55 mM anhydrous sodium sulfate was prepared. During the electrodeposition process, a three-electrode system was used, with the heat-treated CF as the working electrode, graphite rod as the counter electrode and saturated calomel electrode (SCE) as the reference electrode. The working electrode was deposited at a constant potential of -1.5 V vs. SCE for 120 s. Finally, the products were rinsed with DI water and dried to obtain $Mn_3O_4/CuO_x/CF$.

Synthesis of Mn_3O_4/CF

The preparation method was similar to $Mn_3O_4/CuO_x/CF$, except CF was used as the working electrode.

Synthesis of CuO_x/CF

The preparation method was similar to $Mn_3O_4/CuO_x/CF$, except manganese acetate was

not added to the electrodeposition solution.

Characterizations

The scanning electron microscope (SEM) images were taken with a Hitachi S4800. The transmission electron microscopy (TEM), high-resolution transmission electron microscopy (HR-TEM), and high-angle annular dark-field scanning transmission electron microscopy (HAADF-STEM) and energy-dispersive X-ray spectroscopy (EDX) images were obtained from JEOL JEM-2100. The X-ray diffraction (XRD) was recorded with a Bruker D8 Advance A25 System (λ = 0.15468 nm). X-ray photoelectron spectroscopy (XPS) spectra were performed on a Thermofisher K-alpha system using monochromatic Al Kα radiation. All binding energies were referenced to the C 1s peak at 284.8 eV. Ultraviolet photoelectron spectroscopy (UPS) measurements were carried out under a monochromatic light source of He I (21.2 eV). Electron paramagnetic resonance (EPR) spectra were obtained from the Bruker A300 to detect oxygen vacancies. The ultraviolet-visible (UV-Vis) absorbance spectra were measured by a Thermo evolution 300 spectrophotometer. The isotope labeling experiments were measured using ^{1}H NMR (Bruker AVANCE AV 400MHz system).

Electrochemical measurements

Measurements for electrocatalytic reduction of nitrate to ammonia were performed in an H-type electrolytic cell separated by a Nafion 117 membrane using a CHI760E electrochemical workstation (Chen Hua, Shanghai). A three-electrode system was composed of the prepared Mn_3O_4/CuO_x/CF, CuO_x/CF and Mn_3O_4/CF working electrodes (effective surface area: 1 × 1 cm^2), SCE reference electrode and platinum foil counter electrode. 0.5 M Na_2SO_4 solution was evenly distributed to the cathode and anode compartments, and $NaNO_3$ (containing 200 ppm of NO_3^--N) was added to the cathode compartment for electroreduction. Linear sweep voltammetry (LSV) curves were performed at a scan rate of 10 mV s^{-1} in the above electrolyte until the polarization curves reached a steady state. Then, under different potentials, potentiostatic tests for 2 h were performed to evaluate the electrocatalytic performance. Electrochemical impedance spectroscopy (EIS) was recorded in the 0.5 M Na_2SO_4 solution containing 200 ppm of NO_3^--N, varying the frequency from 100 kHz to 0.1 Hz, with an amplitude of 5 mV. The

potential was converted to reversible hydrogen electrode (RHE) potential by the Nernst equation: E (vs. RHE) = E (vs. SCE) + 0.242 + 0.0591 pH.

Determination of ion concentration

Determination of NO_3^--N: Firstly, 0.02 ml electrolyte after electroreduction process was collected and diluted to 5 ml to keep within the detection range. Then, 0.1 mL 1 M HCl and 0.01 mL 0.8 wt% sulfamic acid were added into the above diluted solution and left to stand for 20 min. The absorption spectrum was determined using an ultraviolet-visible (UV-Vis) spectrophotometry, and the absorbances at 220 nm and 275 nm were recorded. According to the equation $A = A_{220nm} - 2A_{275nm}$, the final absorbance was obtained. Concentration-absorbance curve was calibrated with a series of $NaNO_3$ standard solutions.
Determination of NO_2^--N: P-aminobenzenesulfonamide (4 g), N-(1-Naphthyl) ethylenediamine dihydrochloride (0.2 g) and phosphoric acid (10 mL, ρ = 1.70 g/mL) were dissolved in 50 mL ultrapure water to prepare the color reagent. 0.1 ml electrolyte was removed from the electrolytic cell and diluted to 5 ml to keep within the detection range. The color reagent (100 μL) was mixed into the above diluted electrolyte and left to stand for 20 min, and the absorbance at a wavelength of 540 nm was recorded. Concentration-absorbance curve was calibrated with a series of $NaNO_2$ standard solutions.
Determination of NH_3-N: The Nessler reagent was applied as a color reagent to determine the ammonia produced by nitrate reduction. Firstly, 0.1 ml electrolyte after electroreduction process was collected and diluted to 5 ml to keep within the detection range. Then, 0.1 mL potassium sodium tartrate solution (ρ=500 g/L) and 0.1 mL Nessler's reagent were added to the above diluted electrolyte. After sitting for 20 min, the absorbance at a wavelength of 420 nm was recorded. Concentration-absorbance curve was calibrated with a series of NH_4Cl standard solutions.

Isotope labeling experiments

The nitrate reduction isotope labeling experiments were carried out to clarify the ammonia source and quantify the concentration of ammonia using $Na^{15}NO_3$ (99%) as the N-source. 0.5 M Na_2SO_4 solution containing $^{15}NO_3^-$-^{15}N (200 ppm) was added into the cathode compartment for electroreduction. After that, the electrolyte solution containing $^{15}NH_4^+$-^{15}N was extracted, and the pH was adjusted to weak acid with 4 M H_2SO_4. For

further quantification of the ammonia concentration, the calibration curve was obtained by ^{1}H NMR (600 MHz) with an external standard of maleic acid. The method was as follows: First, different concentrations of $^{15}NH_4^+$-^{15}N solutions (50, 100, 150, 200, 250 ppm) and 0.02 g maleic acid were added into 0.5 M Na_2SO_4; Second, 50 μL deuterium oxidized (D_2O) was added in 0.5 mL above mixed solution for the NMR detection; Third, the calibration curve was obtained by using the peak area ratio between $^{15}NH_4^+$-^{15}N and maleic acid. Similarly, the amount of $^{14}NH_4^+$-^{14}N was quantified by this method when $Na^{14}NO_3$ was used as the feeding N-source.

Calculation of the yield, conversion rate, selectivity, and Faraday efficiency

For nitrate electroreduction, the NH_3 yield was calculated by Eq. S1:

$$\text{Yield} = (c_{NH_3} \times V) / (M_{NH_3} \times t \times S) \quad \text{Eq. S1}$$

The conversation rate of NO_3^- (i.e. percentage of NO_3^- concentration participating in the electrochemical reduction reaction to the original NO_3^- concentration) was calculated by Eq. S2:

$$\text{Conversion rate} = \Delta c_{NO_3^-} / c_0 \times 100\% \quad \text{Eq. S2}$$

The selectivity of N_2, NH_3 and NO_2^- (i.e. the percentage of product concentration to NO_3^- concentration participating in the electrochemical reduction reaction) was calculated by Eq. S3:

$$\text{Selectivity} = c / \Delta c_{NO_3^-} \times 100\% \quad \text{Eq. S3}$$

The Faraday efficiency was calculated by Eq. S4:

$$\text{Faraday efficiency} = (8\ F \times c_{NH_3} \times V) / (M_{NH_3} \times Q) \times 100\% \quad \text{Eq. S4}$$

Where c_{NH_3} is the concentration of NH_3 (aq), $\Delta c_{NO_3^-}$ is the concentration difference of NO_3^- before and after electrolysis, c_0 is the initial concentration of NO_3^-, c is the concentration of generated nitrogen, ammonia or nitrite, and V is the electrolyte volume in the cathode compartment (45 mL), M_{NH_3} is the molar mass of NH_3, t is the electrolysis time (2 h), S is the area of the working electrode (1 cm^2), F is the Faraday constant (96485 C mol^{-1}), and Q is the total charge passing the electrode.

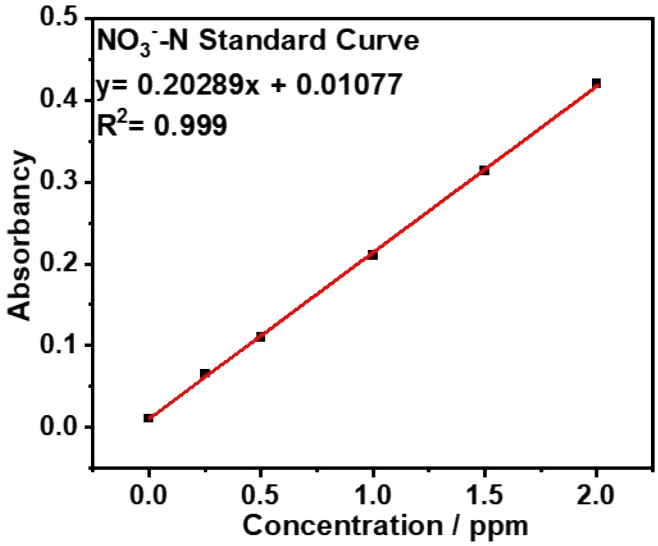

Fig. S1. Calibration curve of NO_3^--N with good linearity.

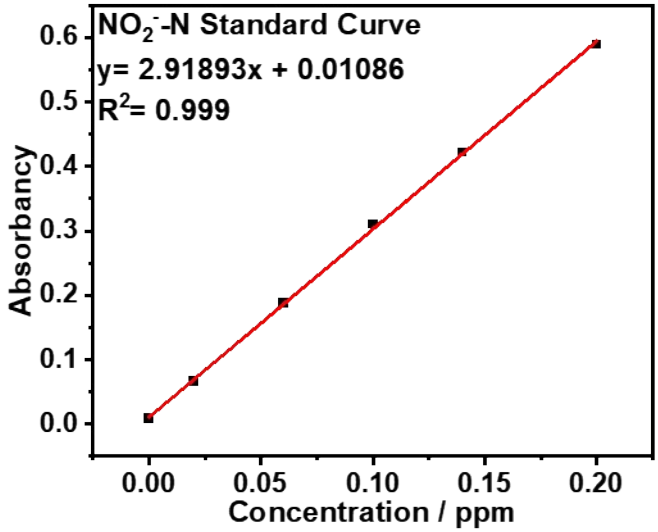

Fig. S2. Calibration curve of NO_2^--N with good linearity.

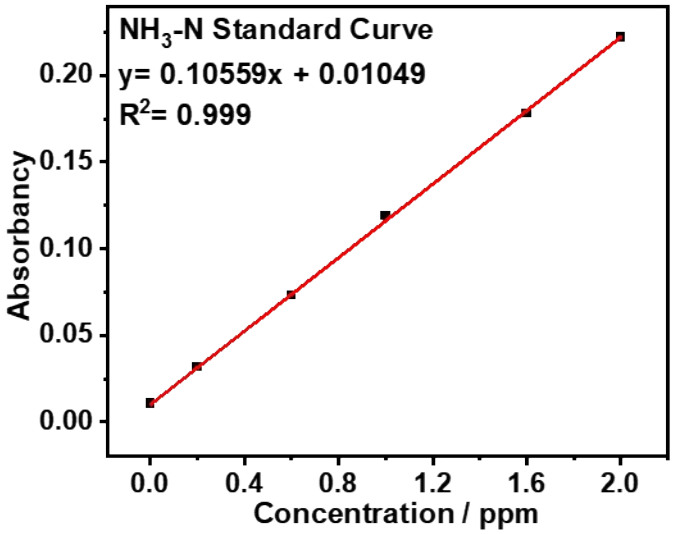

Fig. S3. Calibration curve of NH_3-N with good linearity.

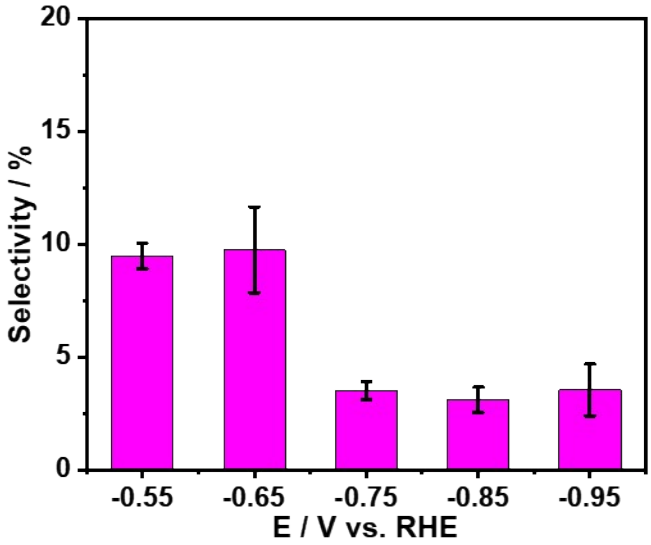

Fig. S4. Selectivity of NO_2^- for Mn_3O_4/CuO_x/CF measured for 2 h under various potentials.

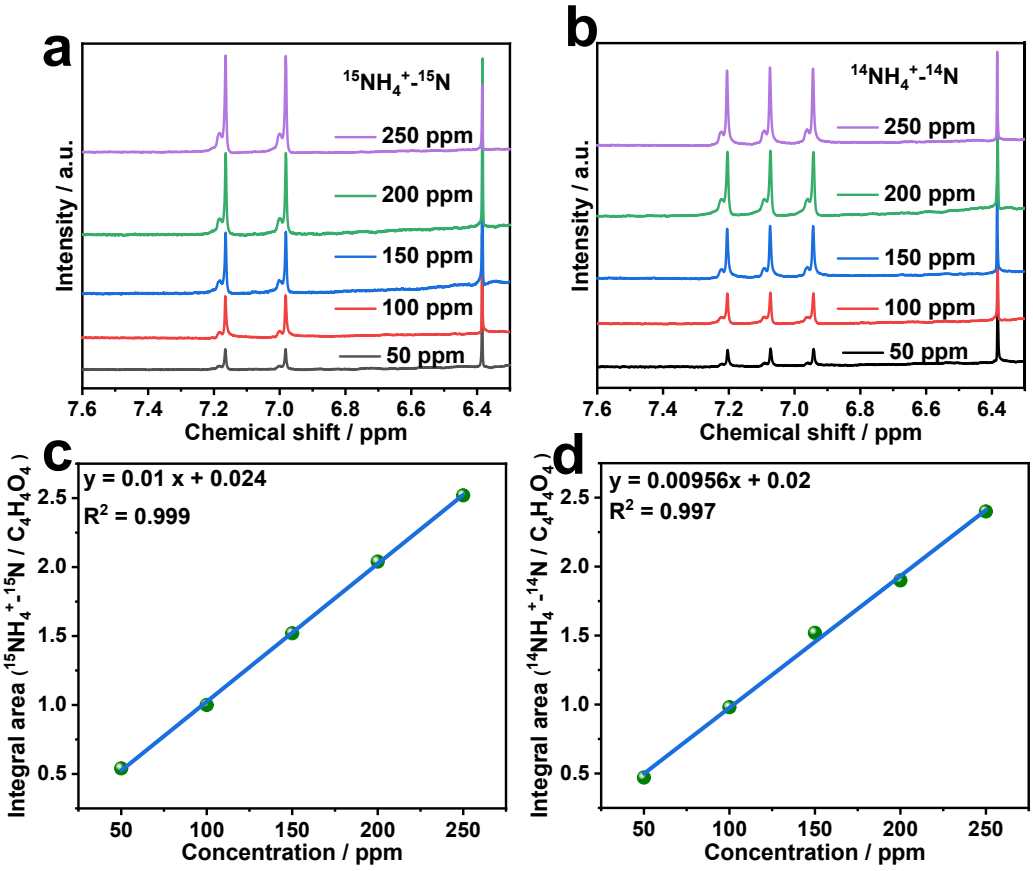

Fig. S5. ^{1}H NMR spectra of (a) $^{15}NH_4^+$-^{15}N and (b) $^{14}NH_4^+$-^{14}N with different concentrations. (c) The standard curve of integral area ($^{15}NH_4^+$-^{15}N/$C_4H_4O_4$) against $^{15}NH_4^+$-^{15}N concentration. (d) The standard curve of integral area ($^{14}NH_4^+$-^{14}N/$C_4H_4O_4$) against $^{14}NH_4^+$-^{14}N concentration.

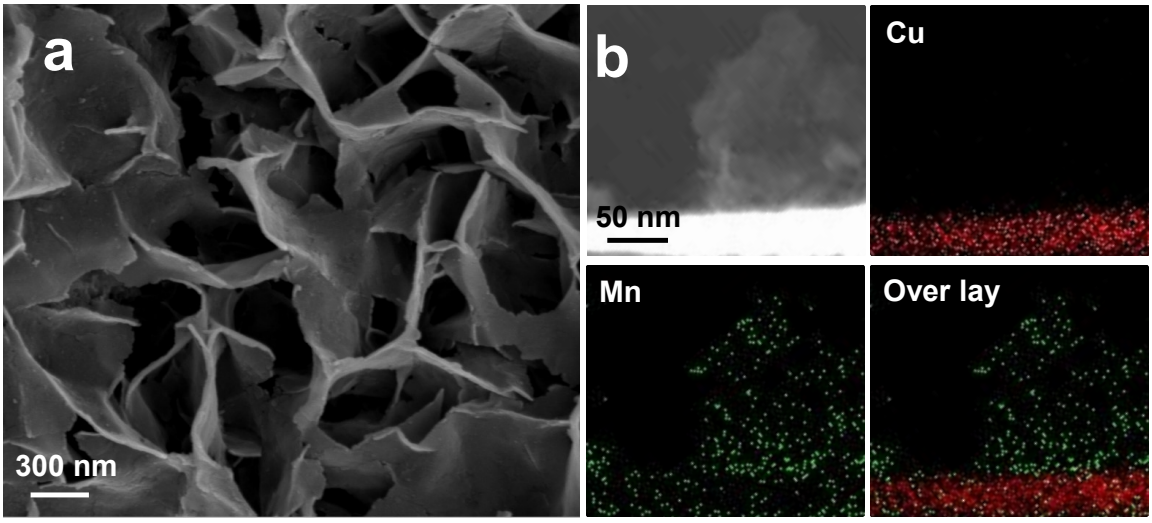

Fig. S6. (a) SEM image and (b) HAADF-STEM image and EDX mapping images of Mn_3O_4/CuO_x/CF after seven cycle tests.

The crossed nanosheet structure and the boundary between the Cu and Mn elements still existed, which proved that the heterostructure could be well preserved after 7 consecutive cycles. (Fig. S6).

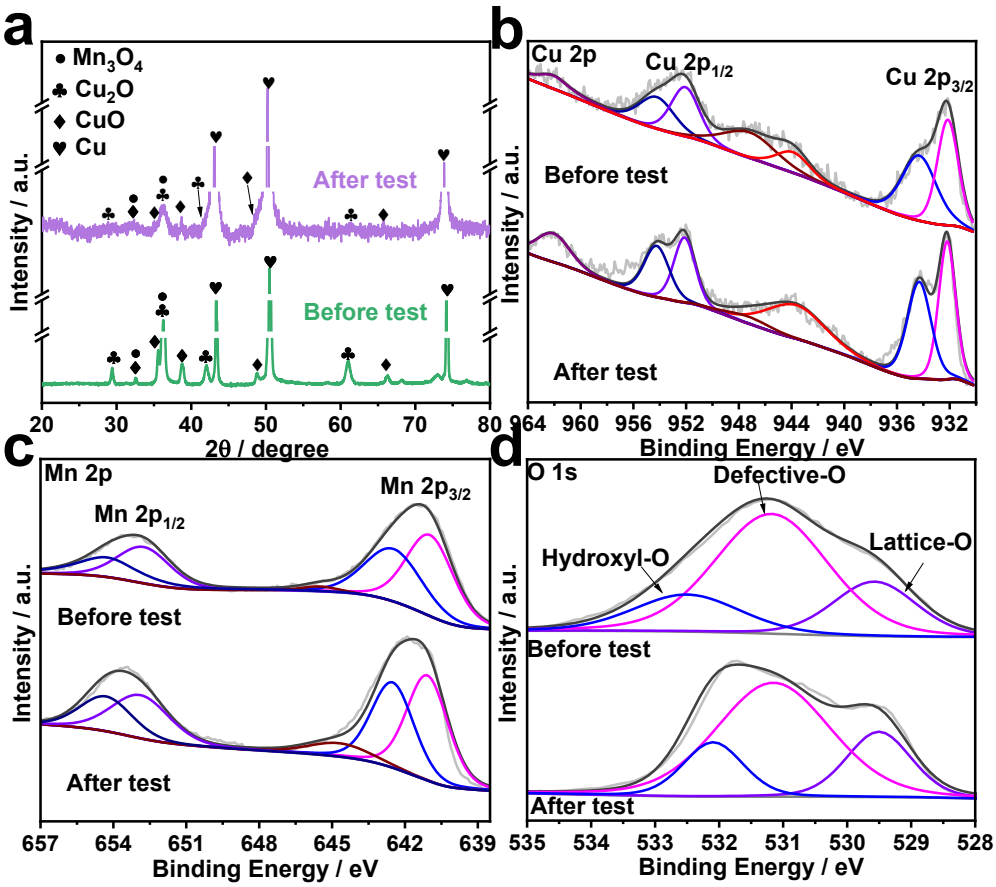

Fig. S7. (a) XRD patterns, (b) Cu 2p XPS spectra, (c) Mn 2p XPS spectra and (d) O 1s XPS spectra of $Mn_3O_4/CuO_x/CF$ before and after test.

In addition, the XRD and XPS characterization results were shown in Fig. S8. Compared with the XRD before the stability testing, the crystallinity of the catalyst decreased. However, the Cu 2p XPS and Mn 2p XPS of $Mn_3O_4/CuO_x/CF$ showed no apparent change before and after the cycle tests. Moreover, the O 1s spectra of $Mn_3O_4/CuO_x/CF$ exhibited that the area percentage of the Defective-O peak after the cycles was not significantly changed (before the reaction: Defective-O/Total-O = 0.62, after 7 consecutive cycles: Defective-O/Total-O = 0.63). These results demonstrated that $Mn_3O_4/CuO_x/CF$ had good electrocatalytic stability.

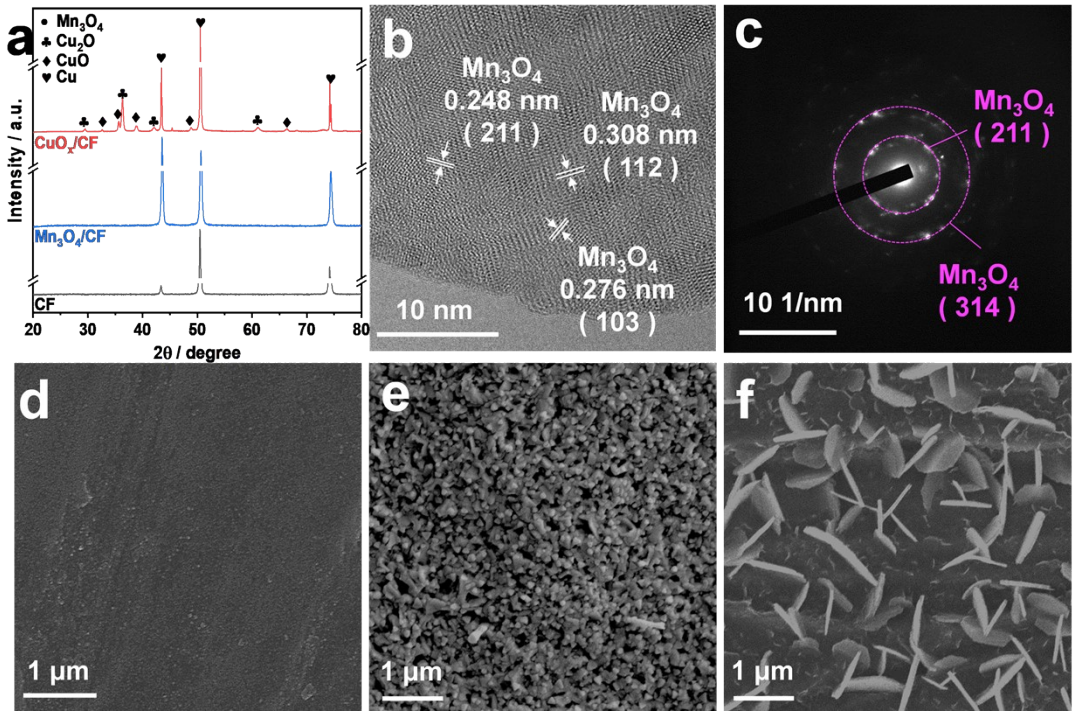

Fig. S8. (a) XRD patterns of CF, Mn_3O_4/CF and CuO_x /CF. (b) HRTEM and (c) SAED pattern of Mn_3O_4/CF. SEM images of (d) CF, (e) CuO_x/CF and (f) Mn_3O_4/CF.

Fig. S8a illustrates the XRD patterns of CuO_x/CF and Mn_3O_4/CF. It can be observed both Cu_2O (JCPDS 05-0667) and CuO (JCPDS 45-0937) species were in the CuO_x/CF. Compared to Mn_3O_4/CF with CF, no obvious Mn_3O_4 diffraction peak was observed. In the HRTEM image of Mn_3O_4/CF (Fig. S8b), the lattice spacings of 0.276, 0.248 and 0.308 nm correspond to (103), (211) and (112) planes of Mn_3O_4 (JCPDS 80-0382).[1,2] In addition, the selected area electron diffraction (SAED) pattern in Fig. S8c showed two obvious diffraction rings, which can be assigned to the (314) and (211) planes of Mn_3O_4.[3] Combining the HRTEM and SAED results, it can be confirmed that Mn_3O_4/CF has been successfully synthesized. Fig S8d-f illustrated the SEM images of CF, CuO_x/CF and Mn_3O_4/CF samples. Prior to the preparation, the CF substrate showed a relatively smooth surface (Fig S8d). In the CuO_x/CF sample, irregular particulates were clearly observed on the CF surface (Fig. S8e). The Mn_3O_4/CF sample exhibited the crossed nanosheet morphology on the CF substrate (Fig. S8f).

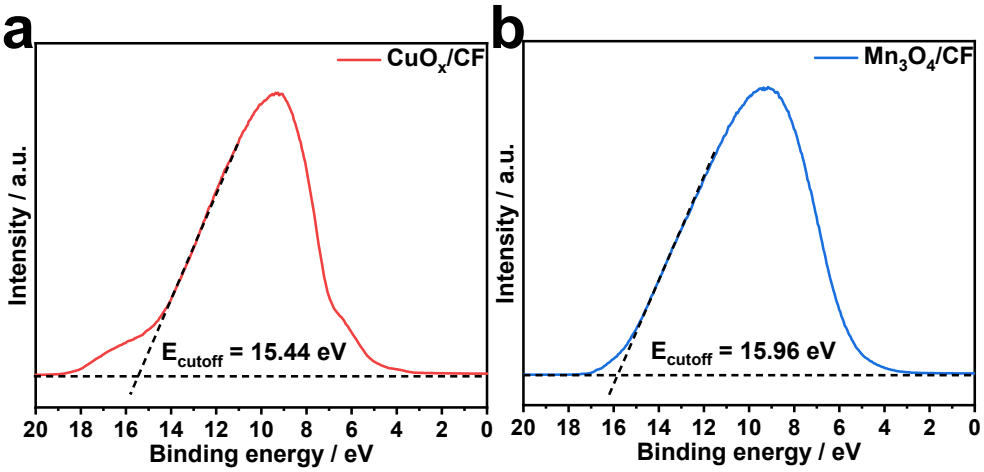

Fig. S9. UPS spectra of (a) CuO_x/CF and (b) Mn_3O_4/CF.

The Fermi energy (E_F) can be determined by subtracting the binding energy of the secondary cutoff edge of the UPS spectra from the He I excitation energy of 21.22 eV, and then the absolute value of its value is the E_F of the sample.

Table S1. Comparison of the quantitative approaches between UV-Vis spectrophotometry and ^{1}H-NMR for nitrate electroreduction at the optimal potential (-0.85 V).

Quantitative method	Nitrogen sources	Detected ions	Concentration
UV-Vis	$^{14}NO_3^-$	$^{14}NH_4^+$ - ^{14}N	141.59 ppm
^{1}H-NMR	$^{14}NO_3^-$	$^{14}NH_4^+$ - ^{14}N	141.21 ppm
^{1}H-NMR	$^{15}NO_3^-$	$^{15}NH_4^+$ - ^{15}N	139.60 ppm

Table S2. The comparison of activity between Mn_3O_4/CuO_x/CF and some other reported electrocatalysts.

Process	Electrocatalysts	Electrolytes	Performance	Ref.
Electroreduction of NO_3^- to NH_3	Mn_3O_4/CuO_x/CF	200 ppm NO_3^--N + 0.5 M Na_2SO_4	S (NH_3): 97.38% FE (NH_3): 87.56%	This work
	Cu@C	1 mM KNO_3 + 1 M KOH	FE (NH_3): 72.0%	4
	FeNPs@MXene	100 ppm NO_3^--N + 0.5 M Na_2SO_4	S (NH_3): 76.8%	5
	Fe SAC	0.5 M KNO_3 + 0.1 M K_2SO_4,	FE (NH_3): ~ 75%	6
	TiO_{2-x}	50 ppm NO_3^--N + 0.5 M Na_2SO_4	S (NH_3):87.1% FE (NH_3): 85.0%	7
	Cu/rGO/graphite plate (GP)	0.02 M $NaNO_3$ + 0.02 M NaCl	S (NH_3): 29.93%	8
	Pd–Cu/γAl_2O_3	50 ppm NO_3^--N	S (NH_3): 19.6%	9
	Cu@$Cu_{2+1}O$ NWs	50 ppm NO_3^--N + 0.5 M K_2SO_4,	S (NH_3): 76%	10
	CuO-Co_3O_4/Ti	100 ppm NO_3^--N + 0.05 M Na_2SO_4	S (NH_3): 44% FE (NH_3): 54.5%	11
	Fe/Cu Composite	100 ppm NO_3^--N + 0.05 M Na_2SO_4	S (NH_3):70%	12
	Co_3O_4-TiO_2-PVP	0.1 M $NaNO_3$ + 0.1 M Na_2SO_4	S (NH_3): 73%	13
	Co_3O_4/Ti	100 ppm NO_3^--N + 0.05 M Na_2SO_4,	S (NH_3): ~ 70%	14

Table S3. The deconvolution result of Cu 2p XPS spectra of $Mn_3O_4/CuO_x/CF$ and CuO_x/CF samples.

Sample	Binding Energy (eV)							
	Cu $2p_{3/2}$				Cu $2p_{1/2}$			
	Cu^+/Cu^0		Cu^{2+}		Cu^+/Cu^0		Cu^{2+}	
	Mean	S.D.	Mean	S.D.	Mean	S.D.	Mean	S.D.
$Mn_3O_4/CuO_x/CF$	932.12	0.03	934.16	0.16	952.04	0.04	954.08	0.17
CuO_x/CF	932.31	0.03	934.20	0.25	952.23	0.03	954.12	0.25

Notes: standard deviation (S.D.)

Table S4. The deconvolution result of Mn 2p XPS spectra of $Mn_3O_4/CuO_x/CF$ and Mn_3O_4/CF samples.

Sample	Binding Energy (eV)							
	Mn $2p_{3/2}$				Mn $2p_{1/2}$			
	Mn^{2+}		Mn^{3+}		Mn^{2+}		Mn^{3+}	
	Mean	S.D.	Mean	S.D.	Mean	S.D.	Mean	S.D.
$Mn_3O_4/CuO_x/CF$	640.95	0.03	642.46	0.02	652.75	0.03	654.26	0.02
Mn_3O_4/CF	640.85	0.02	642.20	0.01	652.65	0.01	654.00	0.01

Notes: standard deviation (S.D.)

Table S5. The deconvolution result of O 1s XPS spectra and the area ratio of Defective-O to Total-O of $Mn_3O_4/CuO_x/CF$, Mn_3O_4/CF and CuO_x/CF samples.

Sample	Binding Energy (eV)						Defective-O/Total-O	
	Lattice-O		Defective-O		Hydroxyl-O			
	Mean	S.D.	Mean	S.D.	Mean	S.D.	Mean	S.D.
$Mn_3O_4/CuO_x/CF$	529.59	0.09	531.24	0.10	532.20	0.10	0.62	0.01

Mn_3O_4/CF	530.86	0.01	531.68	0.03	532.42	0.04	0.45	0.02
CuO_x/CF	529.44	0.04	530.16	0.13	531.74	0.16	0.52	0.01

Notes: standard deviation (S.D.)

References

1 J. Liu, J. Liu, W. Song, F. Wang and Y. Song, *J. Mater. Chem. A*, 2014, **2**, 17477-17488.
2 H. U. Shah, F. Wang, M. S. Javed, N. Shaheen, S. Ali, M. A. Ahmad and K. He, *Mater. Lett.*, 2018, **210**, 148-152.
3 S. Zhu, P. Zhang, L. Chang, Y. Zhong, K. Wang, H. Shao, J. Wang, J. Zhang and C. Cao, *Phys. Chem. Chem. Phys.*, 2016, **18**, 8529-8536.
4 Z. Song, Y. Liu, Y. Zhong, Q. Guo, J. Zeng and Z. Geng, *Adv. Mater.*, 2022, **34**, 2204306.
5 W. J. Sun, L. X. Li, H. Y. Zhang, J. H. He and J. M. Lu, *ACS Sustain. Chem. Eng.*, 2022, **10**, 5958-5965.
6 Z. Y. Wu, M. Karamad, X. Yong, Q. Z. Huang, D. A. Cullen, P. Zhu, C. A. Xia, Q. F. Xiao, M. Shakouri, F. Y. Chen, J. Y. Kim, Y. Xia, K. Heck, Y. F. Hu, M. S. Wong, Q. L. Li, I. Gates, S. Siahrostami and H. T. Wang, *Nat. Commun.*, 2021, **12**, 10.
7 R. Jia, Y. Wang, C. Wang, Y. Ling, Y. Yu and B. Zhang, *ACS Catal.*, 2020, **10**, 3533-3540.
8 E. Rahimi, G. Sajednia, M. Baghdadi and A. Karbassi, *J. Environ. Chem. Eng.*, 2018, **6**, 5249-5258.
9 H. Cheng, P. X. Cui, F. R. Wang, L. X. Ding and H. H. Wang, *Angew. Chem.-Int. Edit.*, 2019, **58**, 15541-15547.
10 T. L. Ren, K. L. Ren, M. Z. Wang, M. Y. Liu, Z. Q. Wang, H. J. Wang, X. N. Li, L. Wang and Y. Xu, *Chem. Eng. J.*, 2021, **426**, 8.
11 M. X. Yang, J. T. Wang, C. D. Shuang and A. M. Li, *Chemosphere*, 2020, **255**, 8.
12 Y. M. Zhang, Y. L. Zhao, Z. Chen, L. Q. Wang, L. C. Zhou, P. P. Wu, F. Wang and P. Ou, *J. Electrochem. Soc.*, 2018, **165**, E420-E428.
13 J. N. Gao, B. Jiang, C. C. Ni, Y. F. Qi, Y. Q. Zhang, N. Oturan and M. A. Oturan, *Appl. Catal. B-Environ.*, 2019, **254**, 391-402.
14 L. H. Su, K. Li, H. B. Zhang, M. H. Fan, D. W. Ying, T. H. Sun, Y. L. Wang and J. P. Jia, *Water Res.*, 2017, **120**, 1-11.